ACS Photonics

Article

pubs.acs.org/journal/apchd5

Rigorous Analysis of Diffraction from Quasicrystalline Gratings via Floquet's Theorem in Higher-Dimensional Space

Farhad A. Namin*[,†] and Douglas H. Werner*[,‡]

[†]Department of Electrical Engineering, Amirkabir University of Technology (Tehran Polytechnic), Tehran, Iran

[‡]Department of Electrical Engineering, The Pennsylvania State University, University Park, Pennsylvania 16802, United States

ABSTRACT: A rigorous approach for the analysis of diffraction from quasicrystalline gratings is presented. Previous methods for determining the diffraction properties of quasicrystalline gratings have relied on periodic supercell approximations. Our method exploits the cut-and-project method, which constructs quasicrystals as irrational slices of higher-dimensional periodic structures onto the physical space. The periodicity in the higher-dimensional space allows for the application of Floquet's theorem. The solutions can then be obtained by solving Maxwell's equations in the higher-dimensional space and projecting the results to the lower dimensional physical space. As an example, the method is applied to a one-dimensional aperiodic grating based on a Fibonacci quasicrystal (QC) where the results that were generated are shown to be in near-perfect agreement with those obtained using the supercell approximations.

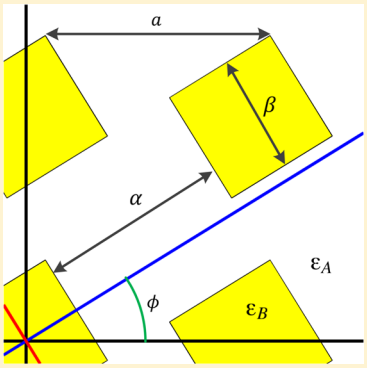

KEYWORDS: *quasicrystals, aperiodic gratings, cut-and-project method, rigorous coupled-wave analysis, Fibonacci grating*

The discovery of quasicrystals (QCs) by Daniel Shechtman was first reported in 1984.[1] Dr. Shechtman had observed 5-fold rotational symmetry in the X-ray diffraction pattern of a metallic solid. The discovery took the field of crystallography by surprise since, according to the crystallographic restriction theorem,[2] 5-fold rotational symmetry was mathematically forbidden in periodic formations and the accepted belief was that all crystals possess translational symmetry. Over the next decade, more observations of forbidden orders of rotational symmetry were reported and scientists also developed the theoretical foundations of QCs.[3−5] Material scientists consider the discovery of QCs one of the most significant and surprising recent developments related to the nature of matter.[1] Dr. Shechtman was awarded the 2011 Nobel Prize in Chemistry "for the discovery of quasicrystals".

In recent years there has been immense interest in the optical and electromagnetic (EM) properties of QCs.[6−10] As noted, QCs lack translational symmetry, but they are deterministic and possess long-range order as well as higher orders of rotational symmetry that are forbidden in periodic lattices.[2] Due to their unique properties, quasicrystalline geometries have been utilized in a wide range of applications such as ultrawideband antenna arrays,[11−13] electronic band gap materials,[14] broadband plasmonic enhancement,[10,15] and surface-enhanced Raman scattering substrates.[8]

A key challenge in evaluating the EM properties of QCs is the lack of analytical tools to accurately and efficiently model them. Traditionally the EM properties of metamaterials and photonic crystals have been evaluated by exploiting their translational symmetry (periodicity). This approach significantly simplifies the analysis by applying periodic boundary conditions and only requiring Maxwell's equations to be solved for one unit cell, rather than the entire structure. As noted, QCs are aperiodic and hence they cannot be modeled accurately using periodic boundary conditions. Currently, the primary analytical method for QCs is the so-called supercell approach. The method essentially takes a large segment of the structure and applies periodic boundary conditions to it.[16] Besides the fact that this approach is very computationally expensive, it can produce inaccurate results since (1) the method attempts to capture an infinite structure in a finite segment and (2) periodicity is artificially introduced into the structure which can lead to spurious modes.

Quasicrystalline geometries are most commonly generated from aperiodic tilings.[17] The Penrose tiling is probably the best known example of an aperiodic tiling with 5-fold rotational symmetry.[2] Once the prototile set of an aperiodic tiling is known, the infinite tiling can be generated either by successively placing prototiles next to each other according to specific matching rules which enforce the aperiodicity of the tiling, or more efficiently by using inflation and substitution rules.[18] A tiling can be converted to a point lattice simply by placing points at the vertices of the tiling. A more rigorous method to generate quasicrystalline geometries is the so-called cut-and-project method.[19] The cut-and-project method generates QC geometries as irrational slices of higher-dimensional periodic crystals. While mathematically more involved, the cut-and-project method provides a greater insight since in the higher-dimensional space, all the properties can be deduced from the unit cell of the hyperlattice. In ref 20, it was proposed

Received: October 6, 2013
Published: February 19, 2014

that this property of QCs can be exploited to solve the field equations in the higher-dimensional space where the structure is periodic and then project the solution onto the real space. As a proof of concept, the method was used to calculate the band diagram of a one-dimensional (1D) Fibonacci photonic QC by applying Bloch's theorem to the higher-dimensional unit cell, where the results were verified using transfer matrix techniques.[20]

In this paper, we expand the higher-dimensional approach to calculate the scattering response of dielectric quasicrystalline gratings. In the higher-dimensional space, the grating is periodic hence Floquet's theorem[21] can be applied. Using the modified version of Maxwell's equations for the higher-dimensional QC, we derive the appropriate boundary value equations to analyze the diffraction response of the QC gratings. Our results in essence permit the analysis of infinite QC gratings using the rigorous coupled-wave analysis (RCWA)[22] method. To verify the validity of our results, we consider a binary 1D dielectric grating based on the Fibonacci QC which can also be obtained as a 1D projection of a two-dimensional (2D) periodic grating. Our results display almost perfect agreement with those obtained using a 1D supercell approximation.

Here, it is important to note that, while we use the concept proposed in ref 20, the problem we are solving is fundamentally different and more complicated. The problem analyzed in ref 20 was determining the spectra of a photonic QC. It was shown that using the cut-and-project method, the problem can be solved by applying Bloch's theorem to the higher dimensional lattice. We use the same concept to analyze diffraction from a quasicrystalline grating, which is a more complicated problem; first, the modes of the grating are obtained by solving the eigen-problem based on the higher dimensional lattice, and then the scattering coefficients are obtained by solving the boundary conditions to match the incident fields to the eigen-modes of the grating. As it will be shown, solving the grating problem requires taking into account all three dimensions of the physical space, whereas in the case of the photonic QCs, only one dimension of the physical space is required.

RESULTS AND DISCUSSION

Cut-and-Project Method. Before giving a description of the cut-and-project method, it is helpful to provide some basic definitions which will be useful later. A crystal is defined as a solid with a discrete diffraction diagram.[2] Mathematically there is a close relationship between diffraction patterns and the Fourier transform. The Dirac delta function introduces a convenient way to represent a set of scatterers as a summation of infinitesimal points. We start by considering $\Lambda = \{\vec{d}_1, \vec{d}_2, ...\}$ as a discrete set of points in E^n, where $\vec{d}_k$ is an n-dimensional vector representing the location of the k-th point in Λ. We can represent this set as the following summation of Dirac delta functions[2]

$$\rho_\Lambda(\vec{x}) = \sum_{\vec{d}_k \in \Lambda} \delta(\vec{x} - \vec{d}_k) \tag{1}$$

The Fourier transform of a function $f(\vec{x})$, $\vec{x} \in R^n$ is denoted by $\hat{f}(\vec{s})$ and defined by the following integral:

$$\hat{f}(\vec{s}) = \int_{R^n} f(\vec{x}) \exp(-2\pi j \vec{x}\cdot\vec{s}) \mathrm{d}\vec{x} \tag{2}$$

where $j = \sqrt{-1}$. It is straightforward to show that the Fourier integral represents a linear operation. Hence, we can denote it by $\mathcal{F}$ and write an equivalent form for eq 2 as

$$\mathcal{F}(f) = \hat{f} \Leftrightarrow \hat{f}(\vec{s}) = \int_{R^n} f(\vec{x}) \exp(-2\pi j \vec{x}\cdot\vec{s}) \mathrm{d}\vec{x} \tag{3}$$

Using the integral in eq 2 it can be shown that $\mathcal{F}(\delta(x - a)) = \exp(-2\pi j a s)$ and from the linearity of $\mathcal{F}$ it follows that the set of points defined in eq 1 has a Fourier transform given by

$$\hat{\rho}_\Lambda(\vec{s}) = \mathcal{F}\left(\sum_{\vec{d}_k \in \Lambda} \delta(\vec{x} - \vec{d}_k)\right) = \sum_{\vec{d}_k \in \Lambda} \exp(-2\pi j \vec{d}_k \cdot \vec{s}) \tag{4}$$

Using eq 4 it can be easily shown that an infinite periodic lattice will have a corresponding spectra in the Fourier domain, which is the sum of Dirac delta functions, and therefore, all solids that contain periodic structure will satisfy the definition of a crystal. A periodic point lattice is said to possess translational symmetry, since a translation mapping by any integer summation of lattice vectors will map the lattice onto itself. Another property associated with crystals is their rotational symmetry. The rotational symmetry of a crystal is defined in terms of the rotational symmetry of its diffraction pattern. Thus, if the diffraction pattern of a point set is unchanged by a $2\pi/n$ rotation, the point set is said to possess n-fold rotational symmetry. Here we note an important theorem regarding periodic lattices in two-dimensional and three-dimensional space (a proof can be found in ref 2):

The Crystallographic Restriction Theorem. Rotational symmetries of order five and those greater than six are impossible for diffraction patterns of periodic lattices existing in two-dimensional and three-dimensional space.

Until the mid 1980s, it was presumed that all crystals possess translational symmetry. In 1982, while studying rapidly solidified aluminum (Al) alloys at Johns Hopkins University, Dr. Dan Shechtman noticed that the electron diffraction pattern of certain Al and manganese (Mn) alloys displayed discrete diffraction and 5-fold rotational symmetry. The discrete diffraction peaks satisfied the definition of a crystal; however, based on the crystallographic restriction theorem, 5-fold rotational symmetry could not be produced by a strictly periodic lattice. He published his results in 1984,[1] which at the time were highly controversial and met with great resistance in the academic community. The main reason for this is because at the time it was assumed that all crystals possessed translational symmetry. In the following years, his results were reconfirmed by other groups and new observations of such solids were made. In later years, this class of materials, which displayed discrete diffraction patterns but lacked periodicity, came to be known as QCs.

A Fibonacci QC is an example of a one-dimensional QC. A Fibonacci sequence can be obtained iteratively from the alphabet set $\{A,B\}$, using the following substitution rule: $A \rightarrow AB$, $B \rightarrow A$. Traditionally, F_n denotes the Fibonacci sequence obtained after n iterative substitutions, starting with $F_0 = B$:[18]

$$\begin{aligned} F_0 &= B \\ F_1 &= A \\ F_2 &= AB \\ F_3 &= ABA \\ &\vdots \end{aligned} \tag{5}$$

dx.doi.org/10.1021/ph400066v | ACS Photonics 2014, 1, 212−220

Generating a Fibonacci point lattice from a Fibonacci sequence is accomplished by assigning a thickness α, β to A and B, respectively, such that $\alpha/\beta = \tau$, where $\tau = (1 + \sqrt{5})/2$ is the golden ratio[2] and placing points at all junctions. Figure 1

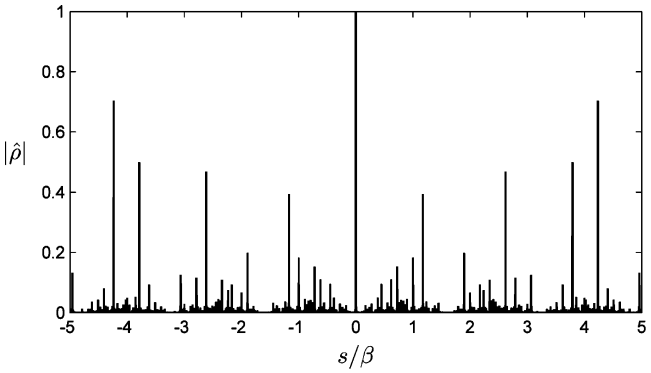

Figure 1. Normalized Fourier transform (magnitude) of a 2585 Fibonacci point lattice corresponding to F_{17}, as defined in eq 5, evaluated using eq 4

shows the normalized Fourier transform (magnitude) of a 2585 Fibonacci point lattice corresponding to F_{17}, as defined in eq 5, evaluated using eq 4. As it can be observed, the Fourier spectrum consists of a weighted sum of discrete peaks, and thus, it satisfies the definition of a crystal.

It is important to note that not all aperiodic, deterministic formations will have discrete Fourier spectra. The Thue-Morse (TM) aperiodic sequence can be obtained iteratively from the alphabet set $\{A,B\}$, using the following substitution rule: $A \rightarrow AB$, $B \rightarrow BA$.[23] A complete description of the TM aperiodic sequence is beyond the scope of this paper and can be found in refs 2, 18, and 19; however, one important property is that, in general, the diffraction pattern is mixed, consisting of a singular continuous spectrum and discrete peaks. The cut-and-project method can only be used to construct aperiodic geometries with discrete diffraction patterns and, thus, cannot be applied to a TM aperiodic sequence. However, it can be applied to two-dimensional QCs such as Penrose and Ammann-Beenker, which have been of great interest for a variety of optical[9] and plasmonic[7,10] applications.

The cut-and-project method[19] constructs a QC lattice in n-dimensional Euclidean space E^n with k-fold rotational symmetry ($k > n$) as an n-dimensional irrational slice of an integer hyperlattice in E^k. The k-dimensional Euclidean space is referred to as the embedding space of the QC.[18] We denote the higher-dimensional space by S^h. In the cut-and-project method, the hyperlattice is projected onto two orthogonal subspaces of dimensions n and $n - k$, which we denote by X and Y, respectively ($S^h = X \oplus Y$). The n-dimensional space X is referred to as the parallel or external subspace and corresponds to the physical space. The $(n - k)$-dimensional space Y is referred to as the perpendicular or internal subspace and corresponds to the unphysical space. The QC can be obtained by taking an n-dimensional slice of the higher-dimensional hyperlattice at a fixed value of Y parallel to X.

Here it is important to note that while it is always possible to embed a QC with k-fold rotational symmetry in E^k, k is not always the minimum dimension for the embedding space. The minimum dimension of the embedding space for a QC with k-fold rotational symmetry k_{min} is

$$k_{min} = \varphi(k) \tag{6}$$

where $\varphi(n)$ is Euler's totient function which is the number of all positive integers less than or equal to n that are relatively prime to n.[18] For example, the Penrose QC has 5-fold rotational symmetry and it can be embedded in a five-dimensional space; however, since $\varphi(5) = 4$, it can also be embedded in the four-dimensional space. The difference lies in the geometry of the unit cells. Embedding a QC with k-fold rotational symmetry in E^k can be simply accomplished using hypercubic orthogonal unit cells, whereas if $k_{min} < k$, the unit cell is nonorthogonal. In the case of the Penrose QC, it can be embedded in the five-dimensional lattice with hypercubic unit cells or in the four-dimensional space with root lattice A_4.[24] A complete description of the cut-and-project method can be found in refs 2, 18, and 19. Here we give a brief description of

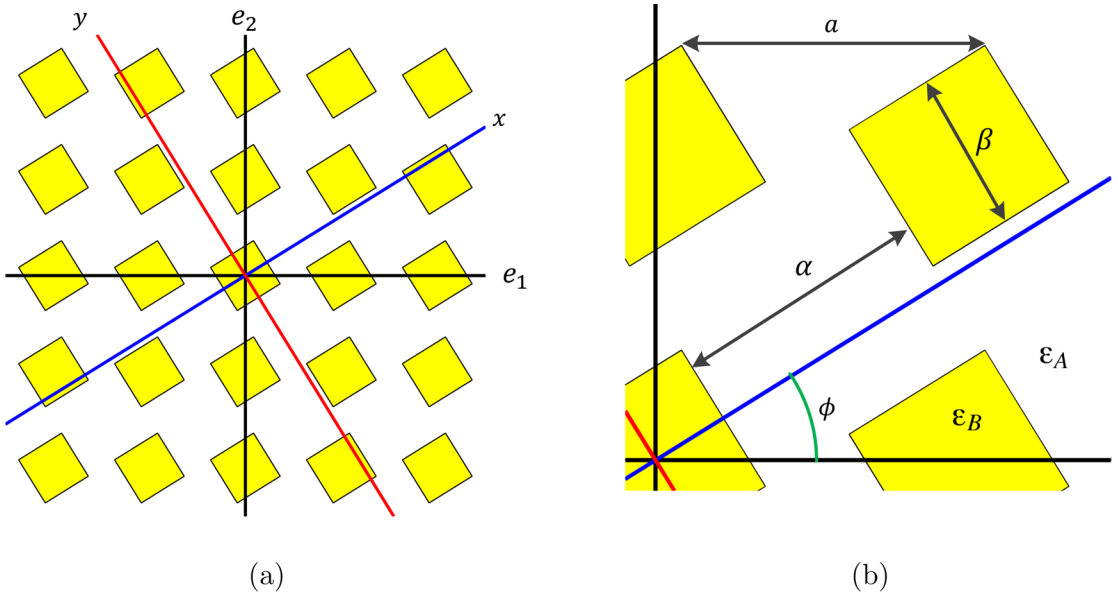

Figure 2. (a) Periodic geometry of the Fibonacci QC in a 2D plane. (b) Structural parameters that define the 2D periodic hyperlattice.

dx.doi.org/10.1021/ph400066v | ACS Photonics 2014, 1, 212−220

the cut-and-project method to generate the 1D Fibonacci QC from a 2D periodic lattice. Generating a Fibonacci QC from a Fibonacci sequence is accomplished by assigning dielectric values ε_A, ε_B and thickness α, β to A and B, respectively, such that $\alpha/\beta = \tau$.[2]

The Fibonacci QC can also be obtained as an irrational slice of a 2D periodic structure. Figure 2a shows the 2D periodic structure that corresponds to the Fibonacci QC. The lattice vectors are $a\hat{\mathbf{e}}_1$ and $a\hat{\mathbf{e}}_2$, where a is the lattice constant and $\hat{\mathbf{e}}_1$ and $\hat{\mathbf{e}}_2$ are unit vectors along e_1 and e_2, respectively. The unit cell is a square with dielectric value ε_A and side a. Inside the unit cell there is a square of dielectric value ε_B and side β rotated at an angle ϕ, where $\tan\phi = 1/\tau$ and

$$\frac{\alpha + \beta}{\sin\phi + \cos\phi} = a \tag{7}$$

Figure 2b shows a close up of a smaller segment of the 2D periodic structure with denoted parameters. To obtain the Fibonacci QC using the cut-and-project method, we start by defining a new orthonormal basis with unit vectors $\hat{\mathbf{x}}$ and $\hat{\mathbf{y}}$ directed along x and y, as shown in Figure 2a. As it can be seen from Figure 2b, the unit vectors $\hat{\mathbf{x}}$ and $\hat{\mathbf{y}}$ are obtained by rotating unit vectors vectors $\hat{\mathbf{e}}_1$ and $\hat{\mathbf{e}}_2$ by an angle ϕ. It can easily be shown that the transformation from the $\hat{\mathbf{e}}_1\hat{\mathbf{e}}_2$ basis to the $\hat{\mathbf{x}}\hat{\mathbf{y}}$ basis can be obtained by the unitary mapping $\mathbf{M}$:

$$\mathbf{M} = \frac{1}{\sqrt{1+\tau^2}}\begin{pmatrix}\tau & 1\\ 1 & -\tau\end{pmatrix} \tag{8}$$

such that

$$\begin{pmatrix}x\\ y\end{pmatrix} = \mathbf{M}\begin{pmatrix}e_1\\ e_2\end{pmatrix} \tag{9}$$

Taking a 1D slice of the 2D structure shown in Figure 2 parallel to $\hat{\mathbf{x}}$ will generate a Fibonacci QC.[25] Since the slice is taken at an angle of ϕ with an irrational slope of $1/\tau$ it will densely fill the unit cell. The value of y at which the slice is taken merely serves as an offset and does not affect the properties of the slice since the slope is not changed.

The general 1D binary quasiperiodic grating diffraction problem is depicted in Figure 3. The Cartesian coordinates

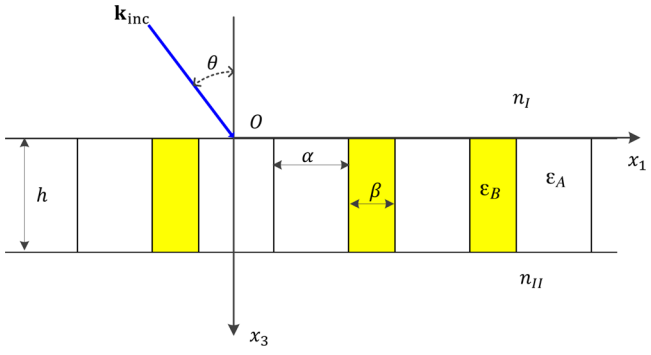

Figure 3. Geometry of scattering from a Fibonacci QC grating.

(with origin denoted by O) of the physical space are represented by (x_1,x_2,x_3) with the corresponding unit vectors $\hat{\mathbf{x}}_1,\hat{\mathbf{x}}_2,\hat{\mathbf{x}}_3$. We consider a quasiperiodic grating based on the Fibonacci sequence with thicknesses α and β and corresponding dielectric values ε_A and ε_B. For simplicity, we assume that all materials in the system have permeability of μ_0. The grating has a thickness of h along x_3 such that $0 \le x_3 \le h$, while the dielectric variation of the grating is along x_1. The grating is bounded by two different media with refractive indices n_I and n_{II}. A linearly polarized EM plane wave from the n_I region is obliquely incident on the grating at an angle of θ. The wave vector for the incident field is

$$\mathbf{k}_{inc} = k_0 n_I[\sin\theta\hat{\mathbf{x}}_1 + \cos\theta\hat{\mathbf{x}}_3] \tag{10}$$

where $k_0 = (2\pi)/(\lambda_0)$ is the free space wavenumber and λ_0 is the free space wavelength. We consider both TE and TM incident waves. The incident electric field for the TE polarized wave is $\mathbf{E}_{inc,TE} = E_{inc,x_2}\hat{\mathbf{x}}_2$, where E_{inc,x_2} is defined as

$$E_{inc,x_2} = \exp[-jk_0 n_I(\sin\theta x_1 + \cos\theta x_3)] \tag{11}$$

We have assumed harmonic fields with $e^{j\omega t}$ time-dependence, where $\omega = 2\pi f$ is the angular frequency. The incident magnetic field for the TM polarized wave is $\mathbf{H}_{inc,TM} = H_{inc,x_2}\hat{\mathbf{x}}_2$, where H_{inc,x_2} is given by

$$H_{inc,x_2} = \exp[-jk_0 n_I(\sin\theta x_1 + \cos\theta x_3)] \tag{12}$$

Maxwell's Equations. In ref 20 it was proposed that the higher-dimensional translational symmetry of QCs can be exploited to evaluate their EM properties. In the higher-dimensional space, the solution domain is reduced to a single unit cell. Since the higher-dimensional unit cell is periodic, it can be analyzed using plane wave expansion methods. The eigenstates of the QC are then obtained by solving Maxwell's equations in the higher-dimensional space. The only difference is the way Maxwell's equations are applied. In the physical space, the source-free time-harmonic wave equations are[26]

$$\nabla \times \mathbf{E} = -j\omega\mu\mathbf{H} \tag{13a}$$

$$\nabla \times \mathbf{H} = j\omega\varepsilon\mathbf{E} \tag{13b}$$

It was shown in ref 20 that higher-dimensional versions of eq 13, which can be applied to periodic hyperlattices are

$$\nabla_{\mathbf{x}} \times \mathbf{E} = -j\omega\mu(\mathbf{x},\mathbf{y})\mathbf{H} \tag{14a}$$

$$\nabla_{\mathbf{x}} \times \mathbf{H} = j\omega\varepsilon(\mathbf{x},\mathbf{y})\mathbf{E} \tag{14b}$$

where $\mathbf{x}$ and $\mathbf{y}$ denote the physical and unphysical dimensions, respectively, and $\nabla_{\mathbf{x}}\times$ denotes the curl operator with respect to the physical coordinates only. The reason for this is that, as noted previously, the value of $\mathbf{y}$ merely acts as an offset and does not alter properties of the slice and hence the eigenvalues of the system. Therefore, eq 14 is not really a higher-dimensional form of the Maxwell's equations since the unphysical coordinates $\mathbf{y}$ act as parameters rather than coordinates.

Equation 14 can be used to evaluate the scattering response of quasicrystalline gratings by applying Floquet's theorem to a single higher-dimensional unit cell. This approach in essence extends the RCWA method to aperiodic quasicrystalline gratings. The derivations of the results for both TE and TM polarizations are shown in the Methods section.

To test the validity of our approach, we can compare the results obtained from applying Floquet's theorem to the 2D periodic hyperlattice with the results obtained using a 1D supercell approximation of the QC. An important question to consider here is how large a supercell must be in order to accurately reflect the properties of the infinite QC. In fact, this is another inadequacy of the supercell approach, since if the

dx.doi.org/10.1021/ph400066v | ACS Photonics 2014, 1, 212−220

structure is not large enough to reflect the long-range order of a QC, then the results will not be accurate. In order to determine the appropriate size for the supercell, we utilized the Fourier transform spectra as a gauge. Figure 4 shows the normalized

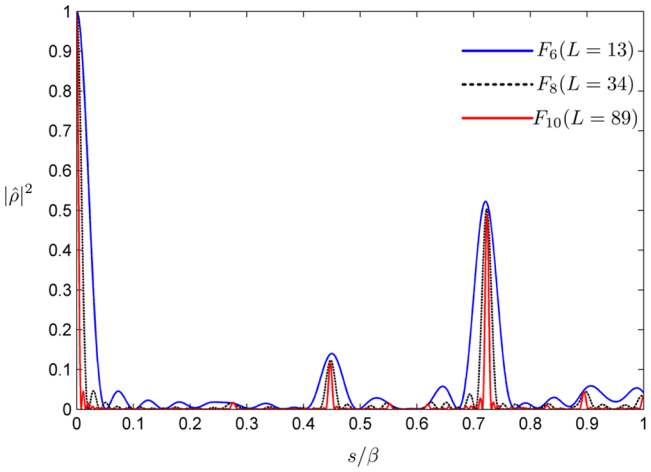

Figure 4. Normalized Fourier spectra (magnitude squared) of Fibonacci point lattices with 13, 34, and 89 layers corresponding, respectively, to F_6, F_8, and F_{10}, as defined in eq 5, calculated using eq 4.

Fourier spectra (magnitude squared) of Fibonacci point lattices with 13, 34, and 89 layers corresponding, respectively, to F_6, F_8, and F_{10}, as defined in eq 5, evaluated using eq 4. Based on these results, we chose F_8 with 34 layers for our supercell simulations since it provided a good trade-off between accuracy and computational complexity. It is worth mentioning that a similar analysis was done in ref 27 for nanoparticle chains based on aperiodic morphologies and they reached a similar conclusion, where it was shown that Fibonacci arrays with as few as 21 particles provided fairly accurate results.

Thus, we consider a Fibonacci supercell consisting of 34 layers, which corresponds to F_8, as defined in eq 5. As outlined previously, the Fibonacci grating is generated from a Fibonacci sequence by assigning dielectric values ε_A, ε_B and thicknesses α, β to A and B such that $\alpha/\beta = \tau$. The total width of the supercell is $W = 21\alpha + 13\beta \approx 25.7a$. The physical setup for all our examples is illustrated in Figure 3.

For our first example, we consider a Fibonacci grating with the parameters $h = (\alpha + \beta)/2$, $\varepsilon_A = 2.15^2$, $\varepsilon_B = 2.4^2$, $n_I = 1$, and $n_{II} = 1.5$. We consider normally incident TE radiation with $1.5a < \lambda_0 < 3a$, where a is the lattice constant of the 2D hyperlattice. To analyze the scattering properties of the supercell, we use the commercially available software package GSolver,[28] which is based on the RCWA algorithm. As it was mentioned before, application of RCWA requires the truncation of infinite series. In order to obtain accurate results for the supercell a large number of terms have to be retained. This is due to the fact that the supercell has a feature size of β which is very small compared to its width ($\beta/W \approx 0.021$). Figure 5 shows the total reflectance of the 1D supercell for three values of M, where M is the maximum order for retained terms, as denoted in eq 21. As it can be seen from the plot, the reflectance spectra does not accurately display all the features for $M = 20$. In order to find the proper value for M we analyzed the 1D supercell with an increasing number of terms. As shown in Figure 5 a high degree of convergence was obtained for $M = 40$ and we did not observe any noticeable improvement for increasing M beyond

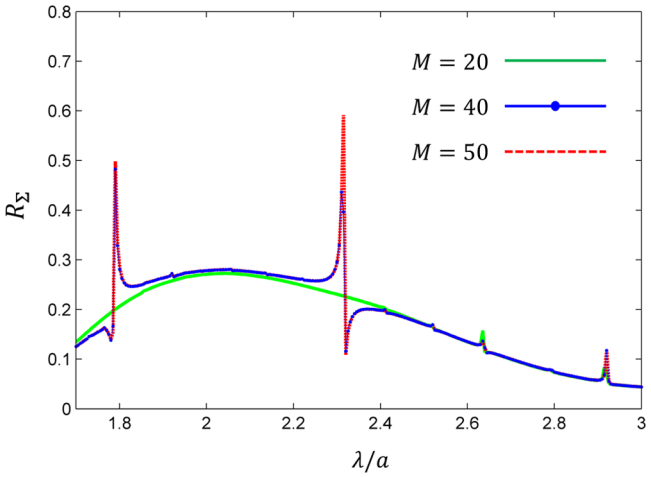

Figure 5. Reflectance spectrum of the 1D Fibonacci supercell evaluated for increasing values of retained terms M.

50. Hence, we used the response for $M = 50$ to compare with the results obtained by applying the Floquet's theorem to the 2D infinite periodic hyperlattice.

Figure 6 shows the total reflectance and transmittance obtained by applying Floquet's theorem to the 2D periodic

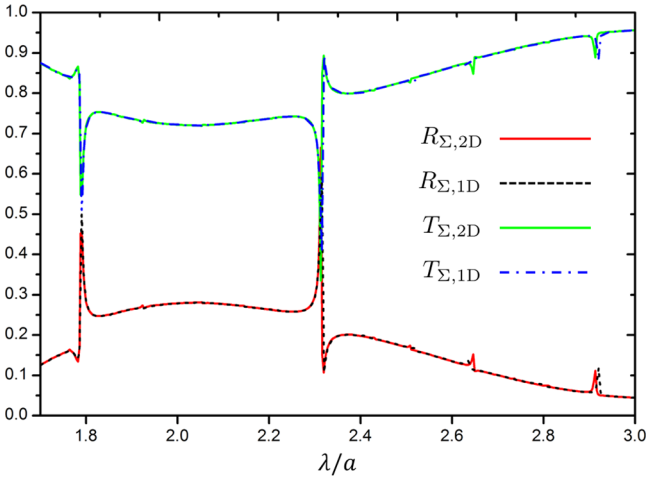

Figure 6. Total reflectance and transmittance obtained by applying Floquet's theorem to the 2D periodic hyperlattice ($R_{\Sigma,2D}$,$T_{\Sigma,2D}$) with $M = 10$ and those obtained by using a 1D supercell periodic approximation ($R_{\Sigma,1D}$,$T_{\Sigma,1D}$) with $M = 50$.

hyperlattice with $M = 10$ and those obtained by using a 1D supercell periodic approximation with $M = 50$. As it can be seen from the plot the results are perfectly matched. It is worth mentioning that retaining a higher order of harmonics which is required for the supercell approximation can lead to numerical instability and convergence issues. Furthermore, for several of our supercell approximations, we had to use quad-precision format to avoid underflow issues, which significantly increased the time and memory requirements.

For the second example, we utilized the periodic hyperlattice approach introduced here to maximize the total reflectance of a Fibonacci grating for a normally incident TM polarized wave with $\lambda/a = 2.75$. The value for n_I was set to unity (i.e., $n_I = 1$) and a binary genetic algorithm with single point crossover[29] was

dx.doi.org/10.1021/ph400066v | ACS Photonics 2014, 1, 212−220

employed to optimize the remaining four parameters, h, ε_A, ε_B, and n_{II}, by minimizing the cost function C defined as

$$C = T_\Sigma \tag{15}$$

where T_Σ is the total reflectance, as defined in eq 34b.

Figure 7 shows the total reflectance and transmittance for the optimized Fibonacci grating obtained by applying Floquet's theorem to the 2D periodic hyperlattice and those obtained by using a 1D supercell periodic approximation. The optimized parameters determined by the genetic algorithm are $h = 0.95a$, $\varepsilon_A = 2.73$, $\varepsilon_B = 5.66$, and $n_{II} = 1.0$. For the supercell calculations, we used the same 34-layer structure as the previous example. Figure 8 shows the reflectance and transmittance of the optimized Fibonacci grating for an oblique incident angle of $\theta = 5°$. As before, to verify our results we have also evaluated the response using the supercell approximation. As it can be seen from Figures 7 and 8, there is excellent agreement between the results generated by applying the Floquet's theorem to the periodic 2D hyperlattice and those obtained by using a 1D supercell approximation.

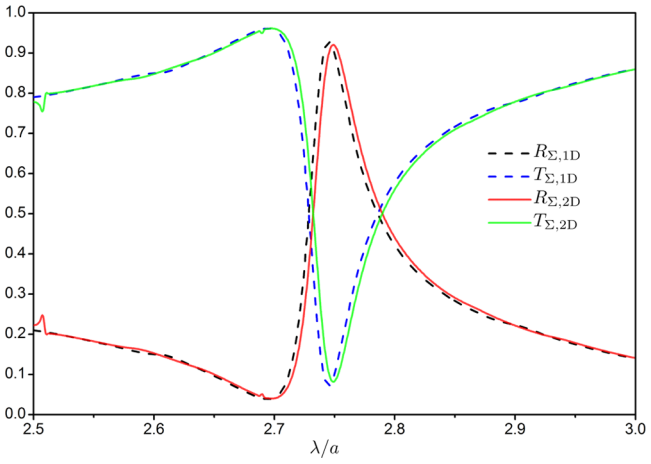

Figure 7. Reflectance and transmittance (TM) of the optimized Fibonacci grating for maximum reflectance at $\lambda/a = 2.75$ obtained from the 2D periodic hyperlattice ($R_{\Sigma,2D}$,$T_{\Sigma,2D}$) and using the 1D supercell periodic approximation ($R_{\Sigma,1D}$,$T_{\Sigma,1D}$) for validation.

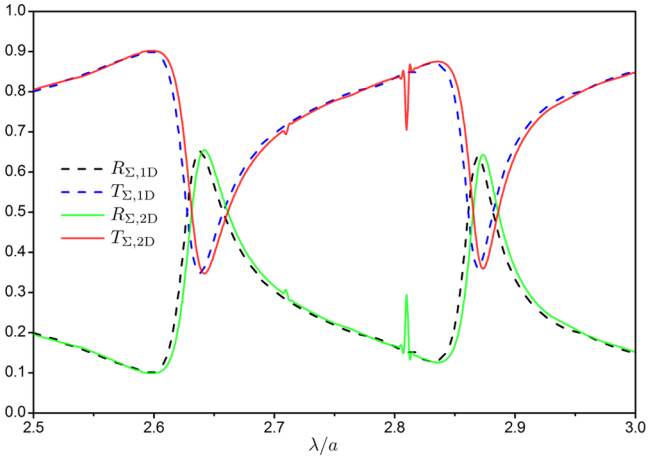

Figure 8. Reflectance and transmittance (TM) of the optimized Fibonacci grating for an oblique incident angle of $\theta = 5°$ obtained from the 2D periodic hyperlattice ($R_{\Sigma,2D}$,$T_{\Sigma,2D}$) and using the 1D supercell periodic approximation ($R_{\Sigma,1D}$,$T_{\Sigma,1D}$) for validation.

METHODS

RCWA for Quasicrystals. RCWA is a widely used method for accurately predicting the diffraction of EM waves by periodic structures.[22] The method is based on Floquet's theorem and Fourier expansion of the fields in the grating region in terms of space harmonics and applying boundary conditions to obtain reflection and transmission coefficients for all diffraction modes. In the physical space, QCs cannot be analyzed using Floquet's theorem due to lack of periodicity. However, analyzing QCs in higher-dimensional space allows the application of Floquet's theorem. The 1D Fibonacci QC grating shown in Figure 3 can be obtained using the cut-and project method as shown in Figure 2a by setting $x \equiv x_1$. In order to analyze the scattering response of the QC grating using RCWA, we consider the TE and TM cases separately.

TE Polarization. We start by considering an obliquely incident TE polarized plane wave with an angle of incidence of θ. The incident electric field and wave vector are given in eqs 11 and 10, respectively. As noted earlier, the Fibonacci QC grating can be obtained from the 2D periodic grating shown in Figure 2a by setting $x \equiv x_1$ and fixing the value of y. Since the 2D grating is periodic with lattice vectors $a\mathbf{e}_1$ and $a\mathbf{e}_2$, then the dielectric function can be expanded in terms of a Fourier series:[30]

$$\varepsilon(e_1, e_2) = \sum_{\mathrm{G}} \varepsilon_{\mathrm{G}} \exp(j\mathbf{G}\cdot\mathbf{r}) \tag{16}$$

where $\mathbf{G}$ and $\mathbf{r}$ are defined as

$$\mathbf{G} = \frac{2m\pi}{a}\hat{e}_1 + \frac{2n\pi}{a}\hat{e}_2 \quad m, n \in \mathbb{Z} \tag{17a}$$

$$\mathbf{r} = e_1\hat{e}_1 + e_2\hat{e}_2 \quad e_1, e_2 \in \mathbb{R} \tag{17b}$$

The value of the Fourier harmonic ε_{G} in eq 16 is given by[30]

$$\varepsilon_{\mathrm{G}} = \frac{1}{a^2}\int\int_U \varepsilon(e_1, e_2) \exp(-j\mathbf{G}\cdot\mathbf{r})\mathrm{d}e_1\mathrm{d}e_2 \tag{18}$$

where the integration is performed over the surface of a unit cell (U) and the normalization factor a^2 is the area of the unit cell as shown in Figure 2b. For simplicity and without loss of generality, we assume $a = 1$. Equation 18 may be evaluated using numerical quadrature methods, which can be very computationally expensive particularly since there are multiple integrals and complex variables involved. However, for our problem, it was possible to obtain a closed-form expression for the Fourier harmonics which considerably reduces the computational burden. For the 2D grating shown in Figure 2b, the closed-form expression for the Fourier harmonic ε_G is

$$\varepsilon_{\mathrm{G}} = \begin{cases} \dfrac{\delta_\varepsilon\beta^2 \sin[\beta\pi\kappa(m\tau + n)] \sin[\beta\pi\kappa(m - n\tau)]}{\pi^2\kappa^2(m\tau + n)(m - n\tau)} & \text{if } |\mathbf{G}| \neq 0 \\ \varepsilon_{\mathrm{A}} + \delta_\varepsilon\beta^2 & \text{if } |\mathbf{G}| = 0 \end{cases} \tag{19}$$

where $\kappa = 1/(1 + \tau^2)^{1/2}$ and $\delta_\varepsilon = \varepsilon_{\mathrm{B}} - \varepsilon_{\mathrm{A}}$. The results in eq 19 are obtained by applying a change of variables to eq 18 and evaluating it with respect to an xy basis.

The electric and magnetic fields are also periodic in the 2D hyperlattice and can be expanded in terms of plane waves using Floquet's theorem:

dx.doi.org/10.1021/ph400066v | ACS Photonics 2014, 1, 212−220

$$E_{x_2}(e_1, e_2, x_3) = \sum_G S_G(x_3) e^{-j(k_0 n_1 \sin\theta x_1 - \mathbf{G}\cdot\mathbf{r})} \tag{20a}$$

$$H_{x_1}(e_1, e_2, x_3) = \frac{-j}{\eta_0} \sum_G U_G(x_3) e^{-j(k_0 n_1 \sin\theta x_1 - \mathbf{G}\cdot\mathbf{r})} \tag{20b}$$

where $\eta_0 = (\mu_0/\varepsilon_0)^{1/2}$ is the free space impedance. In the remainder of the paper, for the sake of brevity, we forego writing the argument for S_G and U_G. Unless otherwise stated, it is always assumed that $S_G \equiv S_G(x_3)$ and $U_G \equiv U_G(x_3)$.

Numerical implementation requires that the infinite series in eq 20 be truncated to a finite number of terms. Hence, we use a finite set of reciprocal lattice vectors $\mathbf{G}$ such that

$$\mathbf{G} = \left\{ \frac{2m\pi}{a}\hat{e}_1 + \frac{2n\pi}{a}\hat{e}_2 \middle| \quad |m| \le M, |n| \le M \right\} \tag{21}$$

The appropriate value for the integer M has to be determined based on the features of the unit cell and is generally inversely proportional to its smallest feature size. This is due to the fact that small variations in the spectral domain correspond to high frequency terms.

In order to apply the modified Maxwell's equations defined in eq 14 to eqs 20a and 20b, it is first required that $\mathbf{G}$ and $\mathbf{r}$ be expressed in terms of their parallel and perpendicular components. Using the orthogonal mapping $\mathbf{M}$ from eqs 9 and 8, we rewrite eqs 20a and 20b as

$$E_{x_2}(x_1, y, x_3) = \sum_G S_G e^{-j(k_0 n_1 \sin\theta x_1 - G_{\|} x_1 - G_{\perp} y)} \tag{22a}$$

$$H_{x_1}(x_1, y, x_3) = \frac{-j}{\eta_0} \sum_G U_G e^{-j(k_0 n_1 \sin\theta x_1 - G_{\|} x_1 - G_{\perp} y)} \tag{22b}$$

where $G_{\|}$ and $G_{\perp}$ are projections of $\mathbf{G}$ onto the parallel (x_1) and perpendicular (y) subspaces, respectively. Applying eqs 14a and 14b to eqs 22a and 22b ($\nabla \times$ with respect to x_1,x_3) we obtain

$$\frac{\partial S_G}{\partial x_3} = k_0 U_G \tag{23a}$$

$$\frac{\partial U_G}{\partial x_3} = \frac{|k_0 n_1 \sin\theta - G_{\|}|^2}{k_0} S_G - k_0 \sum_{G'} \varepsilon_{G-G'} S_{G'} \tag{23b}$$

The term $(k_0 n_I \sin\theta - G_{\|})$ corresponds to the physical component of the Floquet wave vector in the grating. Denoting $\beta_G \equiv k_0 n_I \sin\theta - G_{\|}$, the total fields in region I ($x_3 < 0$) with refractive index n_I and region II ($x_3 > h$) with refractive index n_{II} are given by

$$E_{I,x_2} = E_{inc,x_2} + \sum_{\mathbf{G}} R_G \exp[-j(\beta_G x_1 - k_{I,G}^{\perp} x_3)] \tag{24a}$$

$$E_{II,x_2} = \sum_{\mathbf{G}} T_G \exp\{-j[\beta_G x_1 - k_{II,G}^{\perp}(x_3 - h)]\} \tag{24b}$$

where R_G and T_G are reflection and transmission coefficients for diffraction modes associated with the reciprocal lattice vector $\mathbf{G}$ of the 2D periodic hyperlattice given in eq 17a. The terms $k_{I,G}^{\perp}$ and $k_{II,G}^{\perp}$ denote the perpendicular components of the wave vector for reflected and transmitted modes, which are given by

$$k_{I,G}^{\perp} = \sqrt{n_I^2 k_0^2 - \beta_G^2} \tag{25a}$$

$$k_{II,G}^{\perp} = \sqrt{n_{II}^2 k_0^2 - \beta_G^2} \tag{25b}$$

Note that in order for reflected(transmitted) modes to be propagating, $k_{I,G}^{\perp}$ ($k_{II,G}^{\perp}$) must be real, otherwise they correspond to evanescent modes.

To obtain all the reflection and transmission coefficients, we implement a numerically stable and efficient method which was introduced in ref 31. Equations 23a and 23b can be combined and written in matrix form as

$$[\mathbf{A}][\mathbf{S}_G] = \left[\frac{\partial^2 \mathbf{S}_G}{\partial (x_3')^2}\right] \tag{26}$$

where $x_3' = k_0 x_3$ and

$$\mathbf{A} = \mathbf{K}_x^2 - \mathbf{E} \tag{27}$$

In eq 27, $\mathbf{K}_x$ is a diagonal matrix with elements equal to $(\beta_G)/(k_0)$ and $\mathbf{E}$ is a Toeplitz matrix formed from the Fourier series coefficients in eq 16, with the (G,G') element being $\mathbf{E}(G,G') = \varepsilon_{G-G'}$. The next step requires eigen decomposition of $\mathbf{A}$ as $\mathbf{A} = \mathbf{W}\mathbf{\Lambda}\mathbf{W}^{-1}$, where $\mathbf{W}$ is the matrix of eigenvectors associated with $\mathbf{A}$ and $\mathbf{\Lambda}$ is the diagonal matrix of eigenvalues of $\mathbf{A}$. We define the diagonal matrix $\mathbf{Q}$ whose elements are the positive square roots of the eigenvalues of $\mathbf{A}$, ($\mathbf{QQ} = \mathbf{\Lambda}$) and the matrix $\mathbf{V}$ as $\mathbf{V} = \mathbf{WQ}$. The field harmonics inside the grating can be expanded as

$$S_G = \sum_{G'} w_{G,G'}\{c_{G'}^{+} e^{-k_0 q_{G'} x_3} + c_{G'}^{-} e^{k_0 q_{G'}(x_3 - h)}\} \tag{28a}$$

$$U_G = \sum_{G'} v_{G,G'}\{-c_{G'}^{+} e^{-k_0 q_{G'} x_3} + c_{G'}^{-} e^{k_0 q_{G'}(x_3 - h)}\} \tag{28b}$$

where $w_{G,G'}$, $v_{G,G'}$, and $q_{G'}$ correspond to the (G,G') element of $\mathbf{W}$, (G,G') element of $\mathbf{V}$, and the (G',G') element of $\mathbf{Q}$, respectively. The values $c_{G'}^{+}$ and $c_{G'}^{-}$ can be determined by solving the appropriate boundary conditions. Applying boundary conditions at $x_3 = 0$ and $x_3 = h$ leads to

$$\begin{bmatrix} \delta_{G,0} \\ jn_I \cos\theta \delta_{G,0} \end{bmatrix} + \begin{bmatrix} \mathbf{I} \\ -j\mathbf{Y}_I \end{bmatrix}[\mathbf{R}] = \begin{bmatrix} \mathbf{W} & \mathbf{WX} \\ \mathbf{V} & -\mathbf{VX} \end{bmatrix}\begin{bmatrix} \mathbf{c}^{+} \\ \mathbf{c}^{-} \end{bmatrix} \tag{29a}$$

$$\begin{bmatrix} \mathbf{WX} & \mathbf{W} \\ \mathbf{VX} & -\mathbf{V} \end{bmatrix}\begin{bmatrix} \mathbf{c}^{+} \\ \mathbf{c}^{-} \end{bmatrix} = \begin{bmatrix} \mathbf{I} \\ j\mathbf{Y}_{II} \end{bmatrix}[\mathbf{T}] \tag{29b}$$

where δ_{ij} is the Kronecker delta function and $\mathbf{I}$ is the identity matrix. Matrices $\mathbf{X}$, $\mathbf{Y}_I$, and $\mathbf{Y}_{II}$ are diagonal with elements $e^{-k_0 h q_G}$, $(k_{I,G}^{\perp}/k_0)$, and $(k_{II,G}^{\perp}/k_0)$, respectively.

Equations 29a and 29b can be simultaneously solved for $\mathbf{R}$ and $\mathbf{T}$. However, in ref 31, it was suggested that a much more numerically stable approach would be to first analytically eliminate $\mathbf{R}$ and $\mathbf{T}$ from eqs 29a and 29b, solve the resulting system for $\mathbf{c}^{+}$ and $\mathbf{c}^{-}$, and then obtain $\mathbf{R}$ and $\mathbf{T}$ by substituting $\mathbf{c}^{+}$ and $\mathbf{c}^{-}$ into eqs 29a and 29b. Eliminating $\mathbf{R}$ and $\mathbf{T}$ from eqs 29a and 29b leads to the following system:

$$\begin{bmatrix} \mathbf{W} - j\mathbf{Y}_I^{-1}\mathbf{V} & \mathbf{WX} + j\mathbf{Y}_I^{-1}\mathbf{VX} \\ \mathbf{WX} + j\mathbf{Y}_{II}^{-1}\mathbf{VX} & \mathbf{W} - j\mathbf{Y}_{II}^{-1}\mathbf{V} \end{bmatrix}\begin{bmatrix} \mathbf{c}^{+} \\ \mathbf{c}^{-} \end{bmatrix} = \begin{bmatrix} (n_I \cos\theta \mathbf{Y}_I^{-1} + \mathbf{I})\delta_{G,0} \\ 0 \end{bmatrix} \tag{30}$$

dx.doi.org/10.1021/ph400066v | ACS Photonics 2014, 1, 212−220

Once eq 30 is solved for $\mathbf{c}^+$ and $\mathbf{c}^-$, $\mathbf{R}$ and $\mathbf{T}$ can be calculated using

$$\mathbf{R} = -[\delta_{G,0}] + [\mathbf{W}\ \mathbf{W}\mathbf{X}]\begin{bmatrix}\mathbf{c}^+\\ \mathbf{c}^-\end{bmatrix} \tag{31a}$$

$$\mathbf{T} = [\mathbf{W}\mathbf{X}\ \mathbf{W}]\begin{bmatrix}\mathbf{c}^+\\ \mathbf{c}^-\end{bmatrix} \tag{31b}$$

The diffraction efficiencies for the reflected and transmitted modes are defined as[32]

$$\zeta_{\mathrm{I},G} = |R_G|^2 \mathcal{R}\left(\frac{k_{\mathrm{I},G}^{\perp}}{k_0 n_{\mathrm{I}}\cos\theta}\right) \tag{32a}$$

$$\zeta_{\mathrm{II},G} = |T_G|^2 \mathcal{R}\left(\frac{k_{\mathrm{II},G}^{\perp}}{k_0 n_{\mathrm{I}}\cos\theta}\right) \tag{32b}$$

where $\mathcal{R}(x)$ denotes the real part of x. For a lossless grating, conservation of energy requires that

$$\sum_G (\zeta_{\mathrm{I},G} + \zeta_{\mathrm{II},G}) = 1 \tag{33}$$

Finally, the total reflectance R_Σ and the total transmittance T_Σ may be determined by using the following expressions:

$$R_\Sigma = \sum_G \zeta_{\mathrm{I},G} \tag{34a}$$

$$T_\Sigma = \sum_G \zeta_{\mathrm{II},G} \tag{34b}$$

TM Polarization. The steps in the development for the TM case are very similar to those taken in the TE case. The incident magnetic field is given in eq 12. The fields are periodic in the 2D hyperlattice and can be expanded as Floquet modes:

$$H_{x_2}(e_1, e_2, x_3) = \sum_{\mathbf{G}} U_G e^{-j(k_0 n_{\mathrm{I}} \sin\theta x_1 - \mathbf{G}\cdot\mathbf{r})} \tag{35a}$$

$$E_{x_1}(e_1, e_2, x_3) = j\eta_0 \sum_{\mathbf{G}} S_G e^{-j(k_0 n_{\mathrm{I}} \sin\theta x_1 - \mathbf{G}\cdot\mathbf{r})} \tag{35b}$$

Rewriting $\mathbf{G}$ and $\mathbf{r}$ in terms of their parallel (x_1) and perpendicular (y) components and applying eqs 14a and 14b ($\nabla\times$ with respect to x_1,x_3) we obtain a set of coupled wave equations that can then be reduced to the following system:

$$[\mathbf{EB}][\mathbf{U}_G] = \left[\frac{\partial^2 \mathbf{U}_G}{\partial (x_3')^2}\right] \tag{36}$$

where $\mathbf{B} = \mathbf{K}_x\mathbf{E}^{-1}\mathbf{K}_x - \mathbf{I}$ and $\mathbf{E}$ and $\mathbf{K}_x$ are defined as in eq 27. Analogous to the TE case, we start by considering the eigendecomposition of matrix $\mathbf{EB}$ as $\mathbf{EB} = \mathbf{\Omega}\mathbf{\Delta}\mathbf{\Omega}^{-1}$, where $\mathbf{\Omega}$ is the matrix of eigenvectors associated with $\mathbf{EB}$ and $\mathbf{\Delta}$ is the diagonal matrix of eigenvalues of $\mathbf{EB}$. We then define a diagonal matrix $\mathbf{\Theta}$ whose elements are the positive square roots of the eigenvalues of $\mathbf{EB}$ ($\mathbf{\Theta}\mathbf{\Theta} = \mathbf{\Delta}$) and a matrix $\mathbf{\Gamma}$ as $\mathbf{\Gamma} = \mathbf{E}^{-1}\mathbf{\Omega}\mathbf{\Theta}$. The field harmonics inside the grating can be expanded as

$$U_G = \sum_{G'} \Omega_{G,G'}\{c_{G'}^+ e^{-k_0\Theta_{G'}x_3} + c_{G'}^- e^{k_0\Theta_{G'}(x_3-h)}\} \tag{37a}$$

$$S_G = \sum_{G'} \Gamma_{G,G'}\{-c_{G'}^+ e^{-k_0\Theta_{G'}x_3} + c_{G'}^- e^{k_0\Theta_{G'}(x_3-h)}\} \tag{37b}$$

Applying boundary conditions at $x_3 = 0$ and $x_3 = h$ leads to a set of equations that can be simultaneously solved for reflection and transmission coefficients; however, as was the case for TE polarization, a significantly more stable and efficient approach would be to first solve for $\mathbf{c}^+$ and $\mathbf{c}^-$ by analytically eliminating $\mathbf{R}$ and $\mathbf{T}$. We have not included the derivations, but the following system can be obtained by eliminating $\mathbf{R}$ and $\mathbf{T}$ from the boundary condition equations:

$$\begin{bmatrix}\mathbf{\Omega} - j\mathbf{Z_I}^{-1}\mathbf{\Gamma} & \mathbf{\Omega}\mathbf{X} + j\mathbf{Z_I}^{-1}\mathbf{\Gamma}\mathbf{X}\\ \mathbf{\Omega}\mathbf{X} + j\mathbf{Z_{II}}^{-1}\mathbf{\Gamma}\mathbf{X} & \mathbf{\Omega} - j\mathbf{Z_{II}}^{-1}\mathbf{\Gamma}\end{bmatrix}\begin{bmatrix}\mathbf{c}^+\\ \mathbf{c}^-\end{bmatrix} = \begin{bmatrix}\left(\frac{\cos\theta}{n_{\mathrm{I}}}\mathbf{Z_I}^{-1} + \mathbf{I}\right)\delta_{G,0}\\ 0\end{bmatrix} \tag{38}$$

where $\mathbf{X}$ is defined similar to the TE case such that $\mathbf{Z_I}$ and $\mathbf{Z_{II}}$ are diagonal matrices with elements $(k_{\mathrm{I},G}^{\perp}/k_0 n_{\mathrm{I}}^2)$, and $(k_{\mathrm{II},G}^{\perp}/k_0 n_{\mathrm{II}}^2)$, respectively. Once eq 38 is solved for $\mathbf{c}^+$ and $\mathbf{c}^-$, $\mathbf{R}$ and $\mathbf{T}$ can be calculated using

$$\mathbf{R} = -[\delta_{G,0}] + [\mathbf{\Omega}\ \mathbf{\Omega}\mathbf{X}]\begin{bmatrix}\mathbf{c}^+\\ \mathbf{c}^-\end{bmatrix} \tag{39a}$$

$$\mathbf{T} = [\mathbf{\Omega}\mathbf{X}\ \mathbf{\Omega}]\begin{bmatrix}\mathbf{c}^+\\ \mathbf{c}^-\end{bmatrix} \tag{39b}$$

The diffraction efficiencies for reflected and transmitted TM modes are given by[32]

$$\zeta_{\mathrm{I},G} = |R_G|^2 \mathcal{R}\left(\frac{k_{\mathrm{I},G}^{\perp}/n_{\mathrm{I}}^2}{k_0 n_{\mathrm{I}}\cos\theta}\right) \tag{40a}$$

$$\zeta_{\mathrm{II},G} = |T_G|^2 \mathcal{R}\left(\frac{k_{\mathrm{II},G}^{\perp}/n_{\mathrm{II}}^2}{k_0 n_{\mathrm{I}}\cos\theta}\right) \tag{40b}$$

CONCLUSION

We have presented a rigorous method to analyze the scattering properties of aperiodic QCs. The technique is based on the cut-and-project method which models QCs as irrational projections of higher-dimensional periodic hyperlattices onto the physical space. Due to the translational symmetry of the hyperlattice the solution domain is reduced to a single higher-dimensional hypercube.

It was shown that Maxwells equations can be directly applied to the higher-dimensional lattice by treating the unphysical dimensions as parameters rather than spatial coordinates. This is due to the fact that unphysical dimensions merely correspond to an offset parameter for the cut-and-project method and have no effect on the eigenvalues of the physical system.[20] Based on the modified Maxwell's equations and application of Floquet's theorem to the periodic hyperlattice, we derived results for application of the RCWA method to QC gratings. The most significant advantage of our results is that it reflects the properties of the infinite QC grating as opposed to previous methods that approximate QCs as periodic truncated supercells.

As an example, we considered the Fibonacci QC, which can be obtained as a 1D slice of a 2D periodic lattice. Several cases were considered that included both TE and TM polarizations

dx.doi.org/10.1021/ph400066v | ACS Photonics 2014, 1, 212−220

as well as normal and oblique incidence angles. In all cases our results were confirmed by supercell approximations.

AUTHOR INFORMATION

Corresponding Author

*E-mail: farhad.azadinamin@gmail.com; dhw@psu.edu.

Notes

The authors declare no competing financial interest.

ACKNOWLEDGMENTS

This work was partially supported by the NSF MRSEC Grant No. DMR-0820404.

REFERENCES

(1) Shechtman, D.; Blech, I.; Gratias, D.; Cahn, J. W. Metallic Phase with Long-Range Orientational Order and No Translational Symmetry. *Phys. Rev. Lett.* **2013**, *53*, 1951−1953.

(2) Senechal, M. *Quasicrystals and Geometry*; Cambridge University Press: Cambridge, U.K., 1996.

(3) Steinhardt, D. L. P. Quasicrystals. I. Definition and Structure. *Phys. Rev. B* **1986**, *34*, 596−616.

(4) Steinhardt, D. L. P. Quasicrystals. II. Unit-Cell Configurations. *Phys. Rev. B* **1986**, *34*, 617−647.

(5) Steinhardt, P. J., Ostuland, S., Eds. In *The Physics of Quasicrystals*; World Scientific: Teaneck, NJ, 1987.

(6) Vardeny, Z. V.; Nahata, A.; Agrawal, A. Optics of Photonic Quasicrystals. *Nat. Photon.* **2013**, *7*, 177−187.

(7) Bauer, C.; Kobiela, G.; Giessen, H. 2D Quasiperiodic Plasmonic Crystals. *Sci. Rep.* **2012**, *2*, 1−6.

(8) Gopinath, A.; Boriskina, S. V.; Reinhard, B. M.; Negro, L. D. Deterministic Aperiodic Arrays of Metal Nanoparticles for Surface-Enhanced Raman Scattering (SERS). *Opt. Express* **2009**, *17*, 3741−3753.

(9) Matsui, T.; Agrawal, A.; Nahata, A.; Vardeny, Z. V. Transmission Resonances through Aperiodic Arrays of Subwavelength Apertures. *Nature* **2007**, *446*, 517−521.

(10) Gopinath, A.; Boriskina, S. V.; Feng, N.; Reinhard, B. M.; Negro, L. D. Photonic-Plasmonic Scattering Resonances in Deterministic Aperiodic Structures. *Nano Lett.* **2008**, *8*, 2423−2431.

(11) Spence, T. G.; Werner, D. H. Design of Broadband Planar Arrays Based on the Optimization of Aperiodic Tilings. *IEEE Trans. Antennas Propag.* **2008**, *56*, 76−86.

(12) Namin, F.; Petko, J. S.; Werner, D. H. Analysis and Design Optimization of Robust Aperiodic Micro-UAV Swarm-Based Antenna Arrays. *IEEE Trans. Antennas Propag.* **2012**, *60*, 2295−2308.

(13) Gross, F. B., Ed. In *Frontiers in Antennas: Next Generation Design and Engineering*; McGraw-Hill: New York, NY, 2011; Chapter 1.

(14) Villa, A. D.; Galdi, V.; Capolino, F.; Pierro, V.; Enoch, S.; Tayeb, G. A Comparative Study of Representative Categories of EBG Dielectric Quasi-Crystals. *IEEE Antennas Wireless Propagat. Lett.* **2006**, *5*, 331−334.

(15) Namin, F.; Wang, X.; Werner, D. H. Reflection and Transmission Coefficients for Finite-Sized Aperiodic Aggregates of Spheres. *J. Opt. Soc. Am. B* **2013**, *30*, 1008−1016.

(16) Villa, A. D.; Enoch, S.; Tayeb, G.; Pierro, V.; Galdi, V.; Capolino, F. Band Gap Formation and Multiple Scattering in Photonic Quasicrystals with a Penrose-Type Lattice. *Phys. Rev. Lett.* **2005**, *94*, 183903.

(17) Grunbaum, B.; Shephard, G. C. *Tilings and Patterns*; W. H. Freeman: New York, NY, 1990.

(18) Steurer, W.; Deloudi, S. *Crystallography of Quasicrystals: Concepts, Methods and Structures*; Springer: Berlin, Germany, 2009.

(19) Janssen, T.; Chapuis, G.; de Boissieu, M. *Aperiodic Crystals: From Modulated Phases to Quasicrystals*; Oxford University Press: Oxford, U.K., 2007.

(20) Rodriguez, A. W.; McCauley, A. P.; Avniel, Y.; Johnson, S. G. Computation and Visualization of Photonic Quasicrystal Spectra via Bloch's Theorem. *Phys. Rev. B* **2008**, *77*, 104201.

(21) Ishimaru, A. *Electromagnetic Wave Propagation, Radiation, and Scattering*; Prentice-Hall: Englewood Cliffs, NJ, 1991.

(22) Moharam, M. G.; Gaylord, T. K. Rigorous Coupled-Wave Analysis of Planar-Grating Diffraction. *J. Opt. Soc. Am.* **1981**, *71*, 811−818.

(23) Burr, S. A., Andrews, G. E., Eds. In *The Unreasonable Effectiveness of Number Theory*; American Mathematical Society: Orono, ME, 1991.

(24) Baake, M.; Kramer, P.; Schlottmann, M.; Zeidler, D. Planar Patterns with 5-Fold Symmetry as Sections of Periodic Structures in 4-Space. *Int. J. Mod. Phys. B* **1990**, *4*, 2217−2268.

(25) Janot, C. *Quasicrystals*, 2nd ed.; Oxford University Press: New York, NY, 1994.

(26) Balanis, C. A. *Advanced Engineering Electromagnetics*; John Wiley and Sons: Hoboken, NJ, 1989.

(27) Negro, L. D.; Feng, N.; Gopinath, A. Electromagnetic Coupling and Plasmon Localization in Deterministic Aperiodic Arrays. *J. Opt. A: Pure Appl. Opt.* **2006**, *10*, 064013.

(28) *GSolver*, V5.2; Grating Solver Development Company, Allen, TX, 2010.

(29) Haupt, R. L.; Werner, D. H. *Genetic Algorithms in Electromagnetics*; Wiley: Hoboken, NJ, 2007.

(30) Kreyszig, E. *Advanced Engineering Mathematics*, 9th ed.; John Wiley and Sons: Hoboken, NJ, 2006.

(31) Moharam, M. G.; Grann, E. B.; Pommet, D. A.; Gaylord, T. K. Formulation for Stable and Efficient Implementation of the Rigorous Coupled-Wave Analysis of Binary Gratings. *J. Opt. Soc. Am. A* **1995**, *12*, 1068−1076.

(32) Han, S. T.; Tsao, Y. L.; Walser, R. M.; Becker, M. F. Electromagnetic Scattering of Two-Dimensional Surface-Relief Dielectric Gratings. *Appl. Opt.* **1992**, *31*, 2343−2352.

NOTE ADDED AFTER ASAP PUBLICATION

This paper was originally published ASAP on February 28, 2014, prior to receiving all author corrections. The final corrected version was reposted on March 4, 2014.